Methods

Preparation of proteins and antibodies

Plasmids encoding PID were created by amplification of the appropriate DNA fragments, including the Flag sequence, followed by subcloning into either pET-11d or pCB6 vectors. The Flag–PID protein was expressed in BL21 (Lys) cells and purified on an M2 agarose affinity column (Sigma). Anti-PID antisera was raised against a peptide at the N terminus (residues 56–71) crosslinked with keyhole limpet hemocyanin (KLH). The rabbit polyclonal antibody specific for p300-mediated acetylated p53 [α-p53CTD(Ac)] was raised against the acetylated human p53 C-terminal peptide (H-S55GQSTSRH55LMF-OH (where 5 represents acetylated lysine)) conjugated through the added C-terminal cysteine to KLH. Antisera from immunized rabbits was first passed through a column coupled with the unacetylated peptide (H-SKKGQSTSRHKKLMF-OH) to deplete antibodies that react with unacetylated p53. This step was repeated several times to remove completely the antibodies against the unacetylated p53. The flow-through anti-sera were further affinity purified by use of acetylated p53 peptide coupled with agarose beads.

Purification of PID from nuclear extracts

The tagged cells were grown in DMEM medium, and nuclear extracts were prepared as described[17,18]. The nuclear extract prepared from the Flag–HDAC1 cell line was adjusted to 300 mM KCl and 0.2% NP-40 by addition of 3 M KCl and 10% NP-40, and incubated with M2-agrose beads (sigma) at 4 °C for 6 h by rotation. After washing with a buffer BC300 containing 300 mM KCl and 0.2% NP-40, proteins were eluted from beads by incubating at 4 °C for 60 min with BC100/0.2% NP-40 plus 0.5 mg ml^{-1} Flag peptide. For the differential affinity-binding assay, the Flag–HDAC1 complexes were first dissociated at 2 M urea at 4 °C for 2 h, and then dialysed in a buffer BC200 containing 200 mM KCl and 0.2% NP-40 for affinity binding. The GST–p53 affinity column was prepared by immobilizing the GST–p53 protein on glutathione-sepharose beads under very high stringency conditions (1 M KCl, 1% NP-40 and 0.2% Sarkosyl) to avoid possible leaking of the GST–p53 proteins from the column during elution. The affinity column was first washed with the BC200 buffer, then loaded with dissociated Flag–HDAC1 complex proteins. After extensive washing of the beads with BC300/0.2% NP-40, bound proteins were eluted with a buffer containing 1 M KCl, 1% NP-40 and 0.2% Sarkosyl.

p53 deacetylation assay

Acetylated GST–p53 was prepared by p53 acetylation assay as described[10], and further purified on glutathione-sepharose. The ^{14}C-labelled acetylated p53 was incubated with purified PID-associated complex or the control eluate at 30 °C for 1 h in a buffer containing 10 mM phosphate (pH 7.0), 100 mM NaCl, 5 mM $MgCl_2$, 1 mM EDTA, 0.5 mM dithiothreitol, 0.1 mM PMSF and 5% glycerol. The reactions were resolved on SDS–polyacrylamide gel electrophoresis (PAGE) and analysed by Coomassie blue staining and autoradiography.

Received 17 May; accepted 5 October 2000.

1. Levine, A. J. p53, the cellular gatekeeper for growth and division. *Cell* **88,** 323–331 (1997).
2. Prives, C. & Hall, P. A. The p53 pathway. *J. Pathol.* **187,** 112–126 (1999).
3. Giaccia, A. J. & Kastan, M. B. The complexity of p53 modulation: emerging patterns from divergent signals. *Genes Dev.* **12,** 2973–2983 (1998).
4. Yu, J. *et al.* Identification and classification of p53-regulated genes. *Proc. Natl Acad. Sci. USA* **96,** 14517–14522 (1999).
5. Zhang, Y. *et al.* Analysis of NuRD subunits reveals a histone deacetylase core complex and connection with DNA methylation. *Genes Dev.* **13,** 1924–1935 (1999).
6. Wade, P. A. *et al.* Mi-2 complex couples DNA methylation to chromatin remodeling and histone deacetylation. *Nature Genet.* **23,** 62–66 (1999).
7. Futamara, M. *et al.* Molecular cloning, mapping, and characterization of a novel human gene MTA-L1, showing homology to a metastasis associated gene, MTA1. *J. Hum. Genet.* **44,** 52–56 (1999).
8. Sakaguchi, K. *et al.* DNA damage activates p53 through phosphorylation-acetylation cascade. *Genes Dev.* **12,** 2831–2841 (1998).
9. Liu, L. *et al.* p53 sites acetylated in vitro by PCAF and p300 are acetylated in vivo in reponse to DNA damage. *Mol. Cell Biol.* **19,** 1202–1209 (1999).
10. Gu, W. & Roeder, R. G. Activation of p53 sequence-specific DNA binding by acetylation of the p53 C-terminal domain. *Cell* **90,** 595–606 (1997).
11. Gu, W., Shi, X. L. & Roeder, R. G. Synergistic activation of transcription by CBP and p53. *Nature* **387,** 819–823 (1997).
12. Zhang, Y., LeRoy, G., Seelig, H. P., Lane, W. S. & Reinberg, D. The dermatomyositis-specific autoantigen Mi2 is a component of a complex containing histone deacetylase and nucleosome remodeling activities. *Cell* **95,** 279–289 (1998).
13. Xue, Y. *et al.* NURD, a novel complex with both ATP-dependent chromatin-remodeling and histone deacetylase activities. *Mol. Cell* **2,** 851–861 (1998).
14. Tong, J. K., Hassig, C. A., Schnitzler, G. R., Kingston, R. E. & Schreiber, S. L. Chromatin deacetylation by an ATP-dependent nucleosome remodelling complex. *Nature* **395,** 917–921 (1998).
15. Taunton, J., Hassig, C. A. & Schreiber, S. L. A mammalian histone deacetylase related to the yeast transcriptional regulator RPD3p. *Science* **272,** 408–411 (1996).
16. Hassig, C. A. *et al.* A role for histone deacetylase activity in HDAC1-mediated transcriptional repression. *Proc. Natl Acad. Sci. USA* **95,** 3519–3524 (1998).
17. Gu, W. *et al.* A novel human SRB/MED-containing cofactor complex (SMCC) involved in transcription regulation. *Mol. Cell* **3,** 97–108 (1999).
18. Ito, M. *et al.* Identity between TRAP and SMCC complexes indicates novel pathways for the function of nuclear receptors and diverse mammalian activators. *Mol. Cell* **3,** 361–370 (1999).
19. Toh, Y., Pencil, S. D. & Nicolson, G. L. A novel candidate metastasis-associated gene, mta1, differentially expressed in highly metatastic mammary adenocarcinoma cell lines. cDNA cloning, expression, and protein analyses. *J. Biol. Chem.* **269,** 22958–22963 (1994).
20. Toh, Y. *et al.* Overexpression of MTA1 gene in gastrointerstinal carcinomas: correlation with invasion and metastasis. *Int. J. Cancer* **74,** 459–463 (1997).
21. Toh, Y., Kuwano, H., Mori, M., Nicolson, G. L. & Sugimachi, K. Overexpression of metastasis-associated MTA1 mRNA in invasive oesophagal carcinomas. *Br. J. Cancer* **79,** 1723–1726 (1999).
22. Lin, J., Chen, J., Elenbaas, X. & Levine, A. J. Several hydrophobic amino acids in the p53 amino-terminal domain are required for transcriptional activation, binding to mdm-2 and the adenovirus 5 E1b 55-kD protein. *Genes Dev.* **8,** 1235–1246 (1994).
23. Jimenez, G. S. *et al.* A transactivation-deficient mouse model provides insights into Trp53 regulation and function. *Nature Genet.* **26,** 37–43 (2000).
24. Yoshida, M., Horinouchi, S. & Beppu, T. Trichostatin A and trapoxin: Novel chemical probes for the role of histone acetylation in chromatin structure and function. *BioEssays* **5,** 423–430 (1995).
25. Pearson, M. *et al.* PML regulates p53 acetylation and premature senescence induced by oncogenic Ras. *Nature* **406,** 207–210 (2000).
26. Yu, A., Fan, H., Lao, D., Bailey, A. D. & Weiner, A. M. Activation of p53 or loss of the Cockayne syndrome group B repair protein causes metaphase fragility of human U1, U2, and 5S genes. *Mol. Cell* **5,** 801–810 (2000).
27. Amundson, S. A., Nyers, T. G. & Flornace, A. J. Roles for p53 in growth arrest and apoptosis: putting on the brakes after genotoxic stress. *Oncogene* **17,** 3287–3299 (1998).
28. Attardi, L. D. Lowe, S. W., Brugarolas, J. & Jacks, T. Transcriptional activation by p53, but not induction of the p21 gene, is essential for oncogene-mediated apoptosis. *EMBO J.* **15,** 3693–3701 (1996).
29. Haupt, Y., Rowan, S., Shaulian, E., Vousden, K. H. & Oren, M. Induction of apoptosis in HeLa cells by trans-activation deficient p53. *Genes Dev.* **9,** 2170–2183 (1995).
30. Murphy, M. *et al.* Transcriptional repression by wild-type p53 utilizes histone deacetylase, mediated by interaction with mSin3a. *Genes Dev.* **13,** 2490–2501 (1999).

Supplementary information is available on *Nature*'s World-Wide Web site (http://www.nature.com) or as paper copy from the London editorial office of *Nature*.

Acknowledgements

We thank R. Dalla-Favera, R. Baer and B. Tycko for critical discussions, and use of laboratory space and reagents; K. Vousden, B. Vogelstein, A. Levine, M. Oren, Y. Xiong, C. Hassig, S. L. Schreiber, S. Chellappan, G. Lozano and P. P. Pandolfi for antibodies, cell lines and plasmids; J. Qin, W. Wang and Y. Zhang for help; G. Cattoretti and H. Niu for suggestions in apoptosis assays; the sequencing facility of Columbia University Cancer Center for sequencing; F. Huang, M. Li, A. Nikolaev and N. A. Papanikolaou for sharing unpublished data and critical comment; and R.G. Roeder for continuous support and encouragement. This work was supported in part by grants from the NIH/NCI, the American Cancer Society and the Herbert Irving Comprehensive Cancer Center to W.G.

Correspondence and requests for material should be addressed to W.G. (e-mail: wg8@columbia.edu). The GenBank accession number for the PID sequence is AF295807.

Insights into SCF ubiquitin ligases from the structure of the Skp1–Skp2 complex

Brenda A. Schulman*, Andrea C. Carrano†, Philip D. Jeffrey*, Zachary Bowen*, Elspeth R. E. Kinnucan*, Michael S. Finnin*§, Stephen J. Elledge‡§, J. Wade Harper‡, Michele Pagano† & Nikola P. Pavletich*§

** Cellular Biochemistry and Biophysics Program, and § Howard Hughes Medical Institute, Memorial Sloan-Kettering Cancer Center, New York, New York 10021, USA*
† Department of Pathology and Kaplan Comprehensive Cancer Center, NYU Medical Center, New York, New York 10016, USA
‡ Verna and Marrs McLean Department of Biochemistry and § Howard Hughes Medical Institute, Baylor College of Medicine, Houston, Texas 77030, USA

F-box proteins are members of a large family that regulates the cell cycle, the immune response, signalling cascades and developmental programmes by targeting proteins, such as cyclins, cyclin-dependent kinase inhibitors, IκBα and β-catenin, for ubiquitination (reviewed in refs 1–3). F-box proteins are the substrate-recognition components of SCF (Skp1–Cullin–F-box protein) ubiquitin-protein ligases[4,5]. They bind the SCF constant catalytic core by means of the F-box motif interacting with Skp1, and they bind substrates through their variable protein–protein

interaction domains[6]. The large number of F-box proteins is thought to allow ubiquitination of numerous, diverse substrates[6]. Most organisms have several Skp1 family members, but the function of these Skp1 homologues and the rules of recognition between different F-box and Skp1 proteins remain unknown. Here we describe the crystal structure of the human F-box protein Skp2 bound to Skp1. Skp1 recruits the F-box protein through a bipartite interface involving both the F-box and the substrate-recognition domain. The structure raises the possibility that different Skp1 family members evolved to function with different subsets of F-box proteins, and suggests that the F-box protein may not only recruit substrate, but may also position it optimally for the ubiquitination reaction.

The ~40-residue F-box motif is the common feature of F-box proteins[6]. Variable 'linker' sequences connect F-boxes to protein–protein interaction modules, such as leucine-rich repeats (LRRs) or WD-40 repeats, which are thought to bind directly to substrates. The human F-box protein Skp2 has LRRs, and it regulates the G1/S transition in mammalian cells[7,8] by controlling the abundance of the cyclin-dependent kinase inhibitor, $p27^{Kip1}$ (refs 8–11). Here we describe the structure of a Skp1–Skp2 complex that lacks an amino-terminal 100-residue region of unknown function in Skp2, but that promotes ubiquitination of $p27^{Kip2}$ *in vitro* to an extent comparable to that of full-length Skp2 (ref. 9).

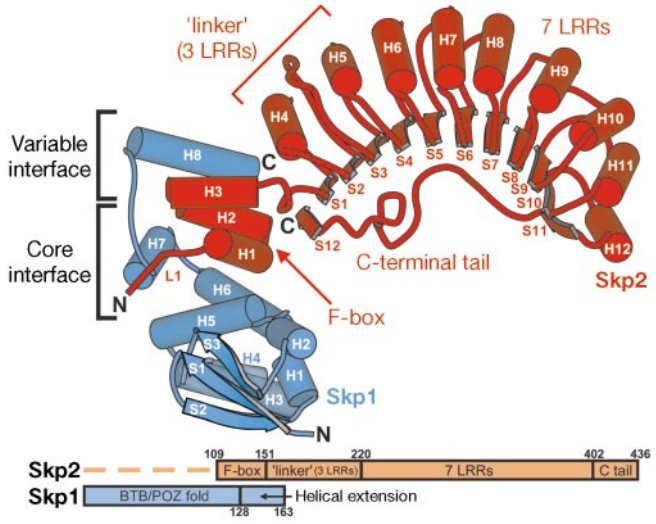

Figure 1 Structure of the Skp1–Skp2 complex. Skp1 is shown in blue and Skp2 is shown in red. The boundaries of the BTB/POZ fold, the C-terminal helical extension of Skp1 and of the F-box, the three non-canonical LRRs, the seven canonical LRRs and the C-terminal tail of Skp2 are shown in the diagram below the structure. The 100-residue N-terminal Skp2 region missing from the crystallized protein is indicated (dashed line). The second LRR has a partially disordered loop instead of the helix characteristic of LRRs.

The structure of the Skp1–Skp2 complex resembles a sickle, with Skp1 and the Skp2 F-box representing the handle and the LRR domain representing the curved blade (Fig. 1). Skp1 has a ~125-residue N-terminal domain with an α/β structure similar to that of the BTB/POZ domain fold[12], but with a helical insertion (H4) and a two-helix carboxy-terminal extension (H7 and H8). The last two helices of the BTB/POZ fold (H5 and H6) and the two helices of the C-terminal extension form the Skp2-binding site (Figs 1 and 2). The structure of the Skp2 F-box consists of three helices, with the H1 helix packing orthogonally with the H2–H3 antiparallel helix pair. The ~70-residue 'linker' following the F-box adopts the structure of three non-canonical LRRs that are contiguous with the seven LRRs predicted from the amino-acid sequence[7]. The ten LRRs, each consisting of a β-strand and an α-helix, pack into a curved structure[13]. They form a single structural domain that is attached directly to the F-box. After the tenth LRR, the ~30-residue C-terminal tail of Skp2 extends back toward the first LRR, packs loosely in the concave surface of the LRR domain and terminates in a short β-strand inserted at the interface between Skp1 and Skp2 (Fig. 1).

The extensive Skp1–Skp2 interface is predominantly hydrophobic and buries a total of 2,980 Å^2 (Figs 1, 3). The interface is interdigitated, with alternating structural elements from Skp1 and Skp2 packing into four layers. The F-box and the Skp1 H8 helix, which are the middle two layers, are sandwiched between the H5, H6 and H7 helices of Skp1 on one side and the first LRR and C-terminal strand of Skp2 on the other side. The interface is best described in two parts from the perspective of the F-box. In one part, one face of the F-box packs with the H5, H6 and H7 helices of Skp1. This is the core interface, as it accounts for two-thirds of the surface area buried (2,050 Å^2) and contains residues conserved in all Skp1 and F-box protein family members (Fig. 3). In the second part, the opposite face of the F-box packs with the H8 helix of Skp1 and also with the first LRR and C-terminal strand of Skp2, burying 930 Å^2 of the surface area. We will refer to this as the variable part of the interface, because the structural elements that the F-box binds here are conserved in Skp1 and Skp2 orthologues, but are not conserved in other F-box and Skp1 family members (such as the 17 Skp1 and 215 F-box sequences in the *Caenorhabditis elegans* genome; Fig. 3). In particular, the Skp1 sequence corresponding to the H8 helix, although highly conserved in Skp1 orthologues (Fig. 2; see also Supplementary Information), is variable in length and sequence among other Skp1 family members in worms, flies and plants. Furthermore, the C-terminal tails of other LRR-containing F-box proteins are also variable in length and sequence, and the portion of the interface corresponding to the first LRR would be different in

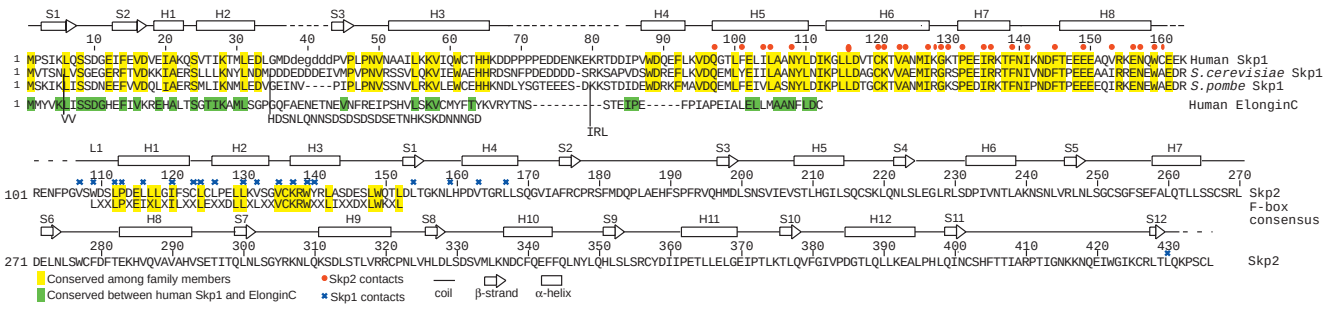

Figure 2 Structural elements and conservation in Skp1 and Skp2. Top, sequence identity between human Skp1 and its orthologues from *S. cerevisiae* and *Schizosaccharomyces pombe* (yellow), and its distant relative, human ElonginC (green). ElonginC is shorter than Skp1, lacking the H4 helix, the last helix of the BTB/POZ fold (H6) and the two-helix C-terminal extension (H7 and H8) of Skp1. Red dots indicate Skp1 residues that contact Skp2; dashed lines indicate disordered segments; lower-case letters denote the internal deletion. Bottom, secondary structure of Skp2, with identity between the Skp2 F-box and the F-box consensus sequence[1,6] (yellow). Blue stars indicate residues that contact Skp1.

non-LRR-containing F-box proteins.

In the core part of the interface, the H5, H6 and H7 helices of Skp1 and the H1, H2 and H3 helices of the F-box pack together in a right-handed superhelical arrangement. The most extensive contacts are made by the L1 loop and H1 helix of the F-box. From the F-box L1 loop, Trp 109, Leu 112 and Pro 113 contact Leu 100, Phe 101, Ile 104, Leu 105, Val 123 and Phe 139 of Skp1 (Figs 2 and 3). From the F-box H1 helix, Leu 116, Ile 120 and Leu 124 contact Ile 104, Leu 105, Leu 116, Cys 120, Val 123 and Ile 127 of Skp1 (Figs 2 and 3). The H2 and H3 F-box helices contribute fewer contacts (Val 132, Val 135 and Trp 139; Figs 2 and 3). Several of the Skp1-contacting F-box residues also have structural functions: Pro 113, a hallmark of the F-box motif, helps to initiate the H1 helix; and Leu 124 and Trp 139 both contribute to the packing of the F-box helices.

The large buried surface area and the extensive intermolecular contacts at the core interface suggest that it is the primary binding site, and explain how an isolated F-box can bind to Skp1 (refs 4, 6, 14, 15). Indeed, the core interface is essentially the same as in the crystal structure of the isolated F-box bound to a truncated Skp1, which lacks the H8 helix (Skp1ΔH8), determined in this study (Table 1). Many of the mutations that disrupt function map to residues in the core[6,16,17] (corresponding to Gly 129, Arg 136 and Ile 141 of Skp1, and to Leu 112, Pro 113, Ile 120, Phe 121 and Leu 124 of the Skp2 F-box). The fact that the F-box and Skp1 residues here are highly conserved in their respective families (Fig. 3) further suggests that the core interface structure will be similar in all combinations of F-box protein and Skp1 family members.

In the variable part of the interface, Skp2 has a large groove formed by residues from the H2 and H3 helices of the F-box (Leu 126, Leu 129, Leu 130, Lys 137, Tyr 140 and Trp 149), the first LRR (Leu 152, Leu 154, Leu 159, Val 163 and Leu 167) and the C-terminal strand (Leu 428 and Leu 430). This groove binds the H8 helix of Skp1 through a combination of van der Waals and hydrogen-bond contacts (to Phe 145, Glu 149, Val 153, Glu 156, Asn 157, Trp 159 and Cys 160 of Skp1; Fig. 3). The most important Skp2 residue in this portion of the interface is Trp 149, which is the only conserved F-box residue here (Fig. 2). Although the side chain of Trp 149 does not contact Skp1, it has a central organizing function at the bottom of the Skp2 groove, packing with residues from the F-box, the first LRR and the C-terminal strand of Skp2. The most important Skp1 residue in this portion of the interface is Trp 159, which is near the end of the Skp1 H8 helix. It binds in the deepest portion of the Skp2 groove, contacting the first LRR, the C-terminal strand and the F-box, and serves as the linchpin for this part of the interface. The importance of the variable interface is highlighted by our finding that the Skp1 H8 helix and Trp 159 are needed for Skp1 function *in vivo*. When we made a mutation corresponding to Trp 159 to alanine or deleted the H8 helix of the *Saccharomyces cerevisiae* Skp1 orthologue, these mutants failed to complement the temperature sensitivity of the *skp1-11* strain (see Supplementary Information).

To test the contribution that this unexpected variable interface makes to the stability of the complex, we used an *in vitro* competition assay to compare the dissociation rates of the Skp2–Skp1 complex with those of the F-box–Skp1ΔH8 complex, which has a core interface structure identical to that of the Skp1–Skp2 complex but that lacks all of the elements unique to the variable interface. The Skp1–Skp2 complex has a half-life greater than 9 h, but the F-box–Skp1ΔH8 complex has a half-life of less than 30 min, indicating that the variable part of the interface contributes substan-

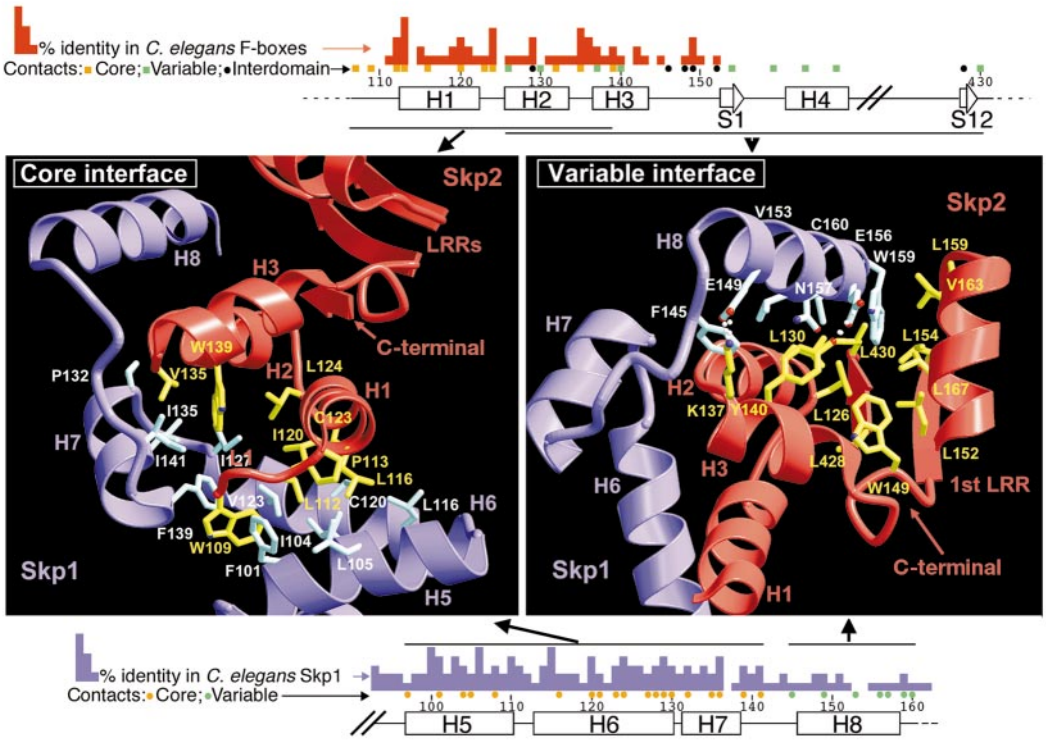

Figure 3 Bipartite Skp1–Skp2 interface. Left, the core interface involves H5, H6 and H7 from Skp1, and L1, H1, H2 and H3 from the F-box. Secondary structures of Skp1 (purple) and Skp2 (red), and side chains of Skp1 (cyan) and Skp2 (yellow) are shown. Right, the variable interface involves H8 from Skp1 and the F-box, first LRR and C-terminal strand from Skp2. White dashes represent hydrogen bonds. Top, conservation of Skp2 residues that make intermolecular contacts to Skp1 in either the core (orange squares) or variable (green squares) parts of the interface, or that make interdomain contacts between the F-box and substrate-binding domain (black dots). Red histogram represents identity among 20 *C. elegans* F-box sequences. Bottom, conservation of Skp1 residues that contact Skp2 in either the core (orange dots) or variable (green dots) parts of the interface (bottom). Violet histogram represents identity among the 17 *C. elegans* Skp1 homologues. Similar histograms are obtained for F-box and Skp1 family members from *D. melanogaster*.

tially to the stability of the complex. This is consistent with studies suggesting that regions outside the F-box enhance association with Skp1 (refs 14, 15, 18).

Although all but one of the Skp1 and Skp2 residues at the second part of the interface are variable in their respective families, several observations suggest that an analogous interface (involving the substrate-binding domain, the F-box and a C-terminal portion of Skp1) will form among most combinations of F-box protein and Skp1 family members, even if the precise structures and residues differ. First, Trp 149 of Skp2 is conserved in both LRR and in non-LRR F-box proteins[6], suggesting that it will couple the F-box and substrate-binding domain in general. Second, the other F-box residues that pack with the Skp1 H8 helix, although not conserved, maintain their overall hydrophobic/hydrogen bonding nature in other F-box proteins. Third, Trp 159 of Skp1 is invariant in orthologues from yeast to humans, suggesting that it will also contact the F-box and substrate-binding domains of non-LRR F-box proteins. Other Skp1 family members contain hydrophobic amino acids near their C termini that may serve analogous functions.

The crystal structure provides a starting point for understanding specificity between different Skp1 and F-box family members. Although *S. cerevisiae* contains a single Skp1, the genomes of higher eukaryotes encode several proteins with homology to most of the Skp1 sequence (S1 to H7). The genomes of *C. elegans* and *Drosophila melanogaster* contain at least 17 and 7 Skp1-like sequences, respectively[19,20]. Although it is not yet known whether these proteins function in SCF-like ubiquitin-protein ligases, our structure suggests that they are close structural homologues of Skp1, except for the C-terminal H8 helix. For example, the cluster of Trp 61, His 65, Trp 88 and Asp 89, which stabilizes the structure through aromatic stacking and a buried hydrogen bond, is invariant in all the fly sequences and highly conserved in the worm sequences, but is entirely absent from other BTB/POZ fold proteins.

Our structure suggests that these Skp1 family members are likely to be functional homologues as well. The strong conservation of the residues in the core portion of the Skp1–Skp2 interface indicates that most of these Skp1 family members should be able to bind to a consensus F-box (Fig. 3). In theory, promiscuous binding between F-box and Skp1 family members would result in combinatorial diversity in the selection and regulation of SCF targets[3]. However, our data suggest that, to provide a complementary structure at the variable portion of the interface, Skp1 family members with divergent C-terminal sequences will preferentially associate with specific subsets of F-box proteins, generating specificity in targeting proteins for degradation.

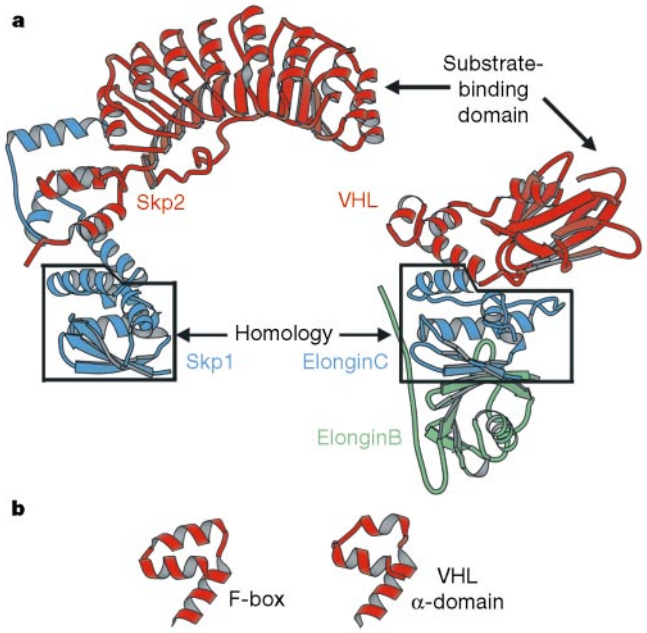

Figure 4 Comparison of the Skp2–Skp1 and VHL–ElonginC–ElonginB complexes. **a**, Homologous portions of Skp1 and ElonginC are aligned and boxed. Skp2 and VHL are red, Skp1 and ElonginC are blue and ElonginB is green. The LRRs of Skp2 (refs 4, 8, 26, 27) and the β-domain of VHL are thought to bind substrate[23]. Owing to its unique C terminus, Skp1 binds the F-box differently from the way that ElonginC binds VHL. The arrangement of helices in the two interfaces is similar, although the helices come from non-corresponding members of the complexes (H1 and H2 from VHL superimpose with H6 and H7 from Skp1, not helices from Skp2). **b**, The ElonginC-binding region of VHL resembles the three-helix cluster structure of the F-box.

Table 1 Statistics from the crystallographic analysis

Protein complex	Skp1–Skp2*	Skp1ΔH8–F-box + LRRs†			Skp1ΔH8–F-box‡		
	Native	Native	Au	Hg	Native	Pt	Hg
Beamline	CHESSA1	NSLSX9B	NSLSX9B	NSLSX9B	NSLSX9B	–	–
Space group	C2	$P2_12_12_1$	$P2_12_12_1$	$P2_12_12_1$	$P2_1$	$P2_1$	$P2_1$
Resolution (Å)	2.8	2.9	3.2	3.5	1.8	2.7	2.4
Observations	598,299	178,486	122,143	87,911	206,639	48,153	65,198
Unique reflections	108,372	23,509	19,152	15,568	29,068	9,847	13,981
Completeness (%) (last shell)	93.7 (93.8)	96.9 (98.7)	95.2 (98.1)	92.6 (95.6)	84.4 (47.1)	96.2 (84.5)	93.5 (83.9)
R_{sym} (%) (last shell)	7.4 (19.4)	8.5 (38.8)	7.6 (36.3)	15.8 (49.7)	3.7 (12.4)	6.0 (18.7)	7.1 (21.8)
$I/\sigma I$ (last shell)	17.9 (5.1)	13.9 (1.9)	18.2 (3.5)	7.9 (2.1)	31.9 (6.7)	19.7 (4.0)	27.6 (6.1)
MIR analysis							
Phasing power			0.72	0.97		1.12	1.45
R_{cullis}			0.90	0.87		0.83	0.74

Refinement statistics							r.m.s.d.		
Protein complex	Resolution (Å)	Reflections	Total atoms	Water atoms	*R*-factor (%) (last shell)	R_{free} (%) (last shell)	Bonds (Å)	Angles (°)	*B* factor (Å)
Skp1–Skp2*	8–2.8	89,527 ($\|F\| > 2\sigma$)	29,168	–	27.5 (35.3)	31.4§ (42.9)	0.010	1.56	2.72
Skp1ΔH8–F-box + LRRS†	20–2.9	23,508 ($\|F\| > 0$)	6,035	–	24.6 (37.8)	28.7 (38.9)	0.012	1.98	2.33
Skp1ΔH8–F-box‡	8–1.8	27,706 ($\|F\| > 0$)	3,336	842	21.8 (28.6)	27.4 (34.3)	0.015	1.89	4.02

$R_{sym} = \Sigma_h \Sigma_i |I_{h,i} - I_h| / \Sigma_h \Sigma_i I_{h,i}$ for the intensity (I) of i observations of reflection h. Phasing power $= \langle F_\lambda \rangle / E$, where $\langle F_\lambda \rangle$ is the r.m.s. heavy atom structure factor and E is the residual lack of closure error. R_{cullis} is the mean residual lack of closure error divided by the dispersive difference. R factor $= \Sigma ||F_{obs}| - |F_{calc}|| / \Sigma |F_{obs}|$, where F_{obs} and F_{calc} are the observed and calculated structure factors, respectively. R_{free} = R factor calculated using 5% of the reflection data chosen randomly and omitted from the start of refinement. r.m.s.d., root-mean-square deviations from ideal geometry and variation in the B factor of bonded atoms.

* Skp(1–37;44–68;84–163)–Skp2(101–436).

† Skp1(1–37;44–147)–Skp2(101–153;194–436).

‡ Skp1(1–37;44–147)–Skp2(101–153).

§ Because of non-merohedral twinning, a minor portion of the data contains contributions from a secondary lattice.

In addition to SCF complexes and their close family members, the VHL von Hippel–Lindau tumor suppressor–ElonginC–ElonginB complex may function in an ubiquitin-protein ligase analogous to the SCF[21,22]. Comparison of the Skp2–Skp1 complex with the structure of the VHL–ElonginC/ElonginB complex[23], however, shows that Skp1 and ElonginC bind their respective Skp2 and VHL partners in different ways (Fig. 4a). Although the structure of the 112-residue ElonginC is similar to the N-terminal two-thirds of Skp1 (Cα r.m.s deviation of 1.27 Å for 74 out of 112 residues), ElonginC lacks the H6, H7 and H8 helices of Skp1 that form the bulk of the Skp2-binding site (Fig. 4a).

The Skp2–Skp1 structure also reveals similarities with the VHL–ElonginC–ElonginB system, which indicate an evolutionary relationship. It reveals (1) that the α-domain of VHL, which mediates most of the binding to ElonginC, has a structure similar to that of the F-box of Skp2 (Fig. 4b); (2) that as in the Skp2 structure, the VHL β-domain, which was proposed to be a substrate-binding domain[23], is tightly coupled to the α-domain; and (3) that the relative positions of the possible substrate-binding domains of Skp2 and VHL and the homologous portions of Skp1 and ElonginC, which may be involved in binding the cullin subunit, are similar (Fig. 4a).

It is not yet understood how the SCF ubiquitinates its substrates. It is possible that the main function of the F-box protein is to recruit the substrate to raise its effective concentration. However, the rigid coupling between the Skp2 substrate-binding domain and Skp1 indicates that the F-box protein may also contribute to the optimal positioning of the substrate for ubiquitination. Although there are no known consensus sequences for ubiquitin-accepting lysines, $p27^{Kip1}$ and IκBα are both ubiquitinated at specific lysine side chains close to their F-box protein-binding sites[24,25]. The selection of lysines for ubiquitination may be determined by the spatial and stereochemical constraints imposed by the tight coupling of the substrate-binding domain with Skp1 and its associated SCF catalytic core.

We do not know how the Skp2 LRR domain binds substrates, but in the LRR-containing proteins RNase inhibitor and U2A′, the concave face of the LRR β-sheet is involved in protein–protein interactions[26,27]. In Skp2, most of the concave face of the LRR domain is filled with a loosely packed 25-residue portion of the Skp2 tail, raising the possibilities that the tail may participate in or regulate substrate binding, or that it may itself be a substrate[3]. On this last possibility, we note that Skp2 protein levels oscillate during the cell cycle[7,18]. Notably, three lysine residues, Lys 416, Lys 417 and Lys 425, in this part of the Skp2 tail protrude away from the structure and may be sites for ubiquitination.

The structure of the Skp1–Skp2 complex provides the first structural insights into the largest class of ubiquitin-protein ligases. It reveals both a general mechanism for F-box protein recruitment to SCF ligases and a second binding site that provides a basis for specificity among family members, and it suggests that the F-box protein may also help position the substrate for the ubiquitination reaction. □

Methods

Protein expression and purification

Three complexes are part of this study. Skp1ΔH8–F-box contains the Skp2 F-box (residues 101–153) and a truncated Skp1 (1–147). Skp1ΔH8–F-box + LRRs contains the same Skp1 mutant and the F-box attached to the seven predicted LRRs (residues 194–409) through an engineered linker. The F-box packs with the third LRR in this structure, but in an artificial manner. We used this complex to determine the structure of the LRR domain to facilitate the structure determination of the Skp1–Skp2 complex that is described here (Table 1). All three structures lack a six-residue internal loop of Skp1 (residues 38–43), which is in a region that we determined to be unstructured on the basis of proteolytic digestion, and is absent from several Skp1 orthologues. The Skp1–Skp2 complex also lacks a protease-sensitive Skp1 loop (residues 71–82) that was present in the Skp1ΔH8–F-box and Skp1ΔH8–F-box + LRRs complexes but that was disordered in these crystal structures. Deletion of either Skp1 loop does not affect binding to either Skp2 or Cul1, as assayed by glutathione *S*-transferase pull-down experiments.

Human Skp2 and Skp1, or their fragments, were cloned as a dicistronic message into the pGEX 4T1 plasmid (Pharmacia)[23], with the GST–Skp2 fusion coding region preceding that of Skp1. Following co-expression in BL21(DE3) at 25 °C, the complexes were purified by glutathione affinity, anion exchange and gel-filtration chromatography and were concentrated by ultrafiltration to ~30–90 mg ml^{-1} in 50 mM Tris-HCl, 150–200 mM NaCl and 5 mM dithiothreitol (DTT), pH 7.6.

Crystallization and structure determination

We grew crystals using the hanging-drop vapour-diffusion method. Crystals of Skp1ΔH8–F-box grew in 36–38% PEG 1500, 0.1 M sodium acetate, pH 4.6, 0.2 M ammonium acetate and 5 mM DTT at 25 °C. They form in the space group $P2_1$ with $a = 46.5$, $b = 41.6$, $c = 87.2$ Å and $\beta = 93.4°$, and have two complexes in the asymmetric unit. Heavy atom soaks were performed in 38% PEG 1500, pH 6.2, supplemented with 3 mM K_2PtCl_4 (3.5 h) or 2.75 mM thimerosal (4 h). Crystals were flash frozen in crystallization buffer containing 43% PEG 1500.

Crystals of Skp1ΔH8–F-box + LRRs grew in 16–18% PEG 4000, 0.1 M Tris-HCl, 0.2 M NaCl and 5 mM DTT, pH 7.4, at 4 °C, by microseeding. They form in the space group $P2_12_12_1$ with $a = 72.6$, $b = 87.0$ and $c = 178.3$ Å, and have two complexes in the asymmetric unit. Heavy atom soaks were performed in 19% PEG 4000, pH 7.4, supplemented with 1 mM $KAu(CN)_2$ (2.5 h) or 0.5 mM thimerosal (4 h). Crystals were flash frozen in crystallization buffer supplemented with 30% ethylene glycol.

Crystals of the Skp1–Skp2 complex were grown in 15–16% PEG 4000, 0.1 M Tris-HCl, 0.2 M ammonium acetate, 10 mM DTT, pH 8.5, at 4 °C, by microseeding and macroseeding. They form in the space group *C*2, with $a = 262.7$, $b = 148.2$, $c = 133.3$ Å and $\beta = 120.0°$, and have eight complexes in the asymmetric unit. These crystals had non-merohedral twinning, producing two closely spaced non-identical diffraction lattices. The combined lattices could be integrated together to yield unit-cell parameters and symmetry consistent with space group *I*222 ($a = 133.4$, $b = 148.2$, $c = 227.6$ Å). The individual lattices are not consistent with *I*222 unit cell parameters (β becomes 90.5°), however, and when integrated separately in space group P1, the data have one exact two-fold symmetry axis (R_{sym} 4.5%) along the direction of the *b* axis and two pseudo-two-fold symmetry axes along *a* and *c* (R_{sym} 25–30%). With only one crystallographic two-fold axis, the appropriate space group is *C*2 with a doubling of the *I*222 asymmetric unit. Most of the spots could be integrated separately with DENZO[28], but presumably some reflections contain minor portions of the secondary lattice. The crystals were flash frozen in crystallization buffer containing 19% PEG 4000 and 30% ethylene glycol.

We processed all data with DENZO[28] and SCALEPACK[28]. For the Skp1ΔH8–F-box and the Skp1ΔH8–F-box + LRRs complexes, multiple isomorphous replacement (MIR) phases were calculated with MLPHARE[29] and were improved by solvent flattening and two-fold non-crystallographic averaging with DM[29] at 2.7 and 3.5 Å, respectively. For the Skp1ΔH8–F-box + LRRs complex, the Skp1–F-box complex was located by molecular replacement with AMORE[29] using the Skp1ΔH8–F-box structure as a search model and the 7-LRR domain was built using the MIR maps. For the structure determination of the Skp1–Skp2 complex, the seven LRRs were first located by molecular replacement using the LRR structure of Skp1ΔH8–F-box + LRRs as a search model. Phases derived from this model were used as the starting point for iterative, eight-fold multidomain non-crystallographic averaging. This allowed for the location of Skp1 and the F-box, and the building of the regions missing in the other two structures. Representative electron density is shown in the Supplementary Information.

All three structures were refined with CNS[30]. The Skp1ΔH8–F-box + LRRs and Skp1–Skp2 structures were refined with two-fold and eight-fold non-crystallographic restraints, respectively, including individual temperature-factor refinement. In the Skp1–Skp2 structure, residue 1, the second engineered linker, residues 161–163 of Skp1 and residues 101–106, 187–189 and 432–436 of Skp2 have no electron density. In addition, residues 184–192 from the second LRR of Skp2 have high temperature factors and are presumably partially disordered. The fraction of residues in the most favoured and additionally allowed regions of the Ramachandran plot, respectively, are 93% and 7% for the Skp1ΔH8–F-box complex, 84% and 16% for the Skp1ΔH8–F-box+LRRs, and 82% and 18% for the Skp1–Skp2 complex. None of these structures has any residues in a disallowed region.

Yeast temperature-sensitivity complementation assay

The *skp1-11* strain has been described[6]. *S. cerevisiae* SKP1 and mutants were expressed under control of the actin promoter in pJP190 (a gift from Z. Zaman), which carries the His marker. Experiments were carried out on SC-His plates. Six independent clones from each transformation were re-streaked, with three incubated each at 25 °C and 37 °C. We analysed 2 μg protein from lysates of yeast grown at 25 °C in SC + glucose-His for the presence of Skp1 (ref. 6).

Skp1 dissociation assay

We mixed 280 μM of the various GST–Skp2–Skp1 complexes with 7.5 mM His-Skp1 (ref. 9). Glutathione *S*-transferase pull-down assays were performed after 0, 0.5, 1, 2, 4, 9 and 24 h. Dissociation was monitored by gel electrophoresis, based on exchange of Skp1 in the starting complex with the slower migrating His-Skp1.

Received 6 June; accepted 4 September 2000.

1. Patton, E. E., Willems, A. R. & Tyers, M. Combinatorial control in ubiquitin-dependent proteolysis: don't Skp the F-box hypothesis. *Trends Genet.* **14,** 236–243 (1998).
2. Koepp, D. M., Harper, J. W. & Elledge, S. J. How the cyclin became a cyclin: regulated proteolysis in the cell cycle. *Cell* **97,** 431–434 (1999).
3. Deshaies, R. J. SCF and Cullin/Ring H2-based ubiquitin ligases. *Annu. Rev. Cell Dev. Biol.* **15,** 435–467 (1999).

4. Skowyra, D., Craig, K. L., Tyers, M., Elledge, S. J. & Harper, J. W. F-box proteins are receptors that recruit phosphorylated substrates to the SCF ubiquitin-ligase complex. *Cell* **91,** 209–219 (1997).
5. Feldman, R. M., Correll, C. C., Kaplan, K. B. & Deshaies, R. J. A complex of Cdc4p, Skp1p, and Cdc53p/cullin catalyzes ubiquitination of the phosphorylated CDK inhibitor Sic1p. *Cell* **91,** 221–230 (1997).
6. Bai, C. *et al.* SKP1 connects cell cycle regulators to the ubiquitin proteolysis machinery through a novel motif, the F-box. *Cell* **86,** 263–274 (1996).
7. Zhang, H., Kobayashi, R., Galaktionov, K. & Beach, D. p19Skp1 and p45Skp2 are essential elements of the cyclin A-CDK2 S phase kinase. *Cell* **82,** 915–925 (1995).
8. Sutterlüty, H. *et al.* p45SKP2 promotes p27Kip1 degradation and induces S phase in quiescent cells. *Nature Cell Biol.* **1,** 207–214 (1999).
9. Carrano, A. C., Eytan, E., Hershko, A. & Pagano, M. SKP2 is required for ubiquitin-mediated degradation of the CDK inhibitor p27. *Nature Cell Biol.* **1,** 193–199 (1999).
10. Tsvetkov, L. M., Yeh, K. H., Lee, S. J., Sun, H. & Zhang, H. p27(Kip1) ubiquitination and degradation is regulated by the SCF(Skp2) complex through phosphorylated Thr187 in p27. *Curr. Biol.* **9,** 661–664 (1999).
11. Nakayama, K. *et al.* Targeted disruption of Skp2 results in accumulation of cyclin E and p27(Kip1), polyploidy and centrosome overduplication. *EMBO J.* **19,** 2069–2081 (2000).
12. Aravind, L. & Koonin, E. V. Fold prediction and evolutionary analysis of the POZ domain: structural and evolutionary relationship with the potassium channel tetramerization domain. *J. Mol. Biol.* **285,** 1353–1361 (1999).
13. Kobe, B. & Deisenhofer, J. Crystal structure of porcine ribonuclease inhibitor, a protein with leucine-rich repeats. *Nature* **366,** 751–756 (1993).
14. Li, F. N. & Johnston, M. Grr1 of *Saccharomyces cerevisiae* is connected to the ubiquitin proteolysis machinery through Skp1: coupling glucose sensing to gene expression and the cell cycle. *EMBO J.* **16,** 5629–5638 (1997).
15. Zhou, P. & Howley, P. M. Ubiquitination and degradation of the substrate recognition subunits of SCF ubiquitin-protein ligases. *Mol. Cell* **2,** 571–580 (1998).
16. Connelly, C. & Hieter, P. Budding yeast SKP1 encodes an evolutionarily conserved kinetochore protein required for cell cycle progression. *Cell* **86,** 275–285 (1996).
17. Russell, I. D., Grancell, A. S. & Sorger, P. K. The unstable F-box protein p58-Ctf13 forms the structural core of the CBF3 kinetochore complex. *J. Cell Biol.* **145,** 933–950 (1999).
18. Lisztwan, J. *et al.* Association of human CUL-1 and ubiquitin-conjugating enzyme CDC34 with the F-box protein p45(SKP2): evidence for evolutionary conservation in the subunit composition of the CDC34-SCF pathway. *EMBO J.* **17,** 368–383 (1998).
19. Costanzo, M. C. *et al.* The yeast proteome database (YPD) and *Caenorhabditis elegans* proteome database (WormPD): comprehensive resources for the organization and comparison of model organism protein information. *Nucleic Acids Res.* **28,** 73–76 (2000).
20. Rubin, G. M. *et al.* Comparative genomics of the eukaryotes. *Science* **287,** 2204–2215 (2000).
21. Lonergan, K. M. *et al.* Regulation of hypoxia-inducible mRNAs by the von Hippel-Lindau tumor suppressor protein requires binding to complexes containing elongins B/C and Cul2. *Mol. Cell. Biol.* **18,** 732–41 (1998).
22. Kamura, T. *et al.* Rbx1, a component of the VHL tumor suppressor complex and SCF ubiquitin ligase. *Science* **284,** 657–661 (1999).
23. Stebbins, C. E., Kaelin, W. G. Jr & Pavletich, N. P. Structure of the VHL-ElonginC-ElonginB complex: implications for VHL tumor suppressor function. *Science* **284,** 455–461 (1999).
24. Shirane, M. *et al.* Down-regulation of p27(Kip1) by two mechanisms, ubiquitin-mediated degradation and proteolytic processing. *J. Biol. Chem.* **274,** 13886–13893 (1999).
25. Spencer, E., Jiang, J. & Chen, Z. J. Signal-induced ubiquitination of IκBα by the F-box protein Slimb/β-TrCP. *Genes Dev.* **13,** 284–294 (1999).
26. Kobe, B. & Deisenhofer, J. A structural basis of the interactions between leucine-rich repeats and protein ligands. *Nature* **374,** 183–186 (1995).
27. Price, S. R., Evans, P. R. & Nagai, K. Crystal structure of the spliceosomal U2B′′–U2A′ protein complex bound to a fragment of U2 small nuclear RNA. *Nature* **394,** 645–650 (1998).
28. Otwinowski, Z. & Minor, W. Processing of X-ray diffraction data collected in oscillation mode. *Methods Enzymol.* **176,** 307–326 (1997).
29. Collaborative Computational Project B. The CCP4 suite: programs for protein crystallography. *Acta Crystallogr. D* **50,** 760–763 (1994).
30. Brünger, A. T. *et al.* Crystallography & NMR system: A new software suite for macromolecular structure determination. *Acta Crystallogr. D* **54,** 905–921 (1998).

Supplementary information is available on *Nature's* World-Wide Web site (http://www.nature.com) or as paper copy from the London editorial office of *Nature*.

Acknowledgements

We thank H. Erdument-Bromage for N-terminal sequence and mass spectroscopic analysis; P. Sorger for communication of results before publication; A. Ansari, P. Murray and members of the Pavletich lab for discussions; C. Murray for administrative assistance; and the staff of the National Synchotron Light Source X9B beamline and of the Cornell High Energy Synchotron Source MacChess for help with data collection. B.A.S. was supported by a Foundation for Advanced Cancer Studies fellowship from the Life Sciences Research Foundation. This work was supported by the NIH, the Howard Hughes Medical Institute, the Dewitt Wallace Foundation, the Samuel and May Rudin Foundation, the Human Frontiers Science Program and the Welch Foundation.

Correspondence and requests for materials should be addressed to N.P.P. (e-mail: Nikola@xray2.mskcc.org). Coordinates have been deposited in the Protein Data Bank (under accession codes 1FS1 (Skp1ΔH8–F-box), 1FS2 (Skp1ΔH8–F-box+LRRs) and 1FQV (Skp1–Skp2)).